One-dimensional Droplet Model for Prediction of Jet-tip Height of Subcooling Mixing Jet for Cryogenic Propellant Storage Tank

Osamu Kawanami (kawanami@eng.u-hyogo.ac.jp)
University of Hyogo
Kentaro Takeda
University of Hyogo
Ryoki Matsushima
University of Hyogo
Ryoji Imai
Muroran Institute of Technology
Yutaka Umemura
Japan Aerospace Exploration Agency
Takehiro Himeno
University of Tokyo

Research Article

Keywords: One-dimensional Droplet Model , Prediction of Jet-tip Height, Subcooling Mixing Jet, Cryogenic Propellant Storage Tank

Posted Date: September 29th, 2021

DOI: https://doi.org/10.21203/rs.3.rs-929364/v1

One-dimensional droplet model for prediction of jet-tip height of subcooling mixing jet for cryogenic propellant storage tank

Osamu Kawanami[1,*], Kentaro Takeda[1], Ryoki Matsushima[1], Ryoji Imai[2,+], Yutaka Umemura[3,+], and Takehiro Himeno[4,+]

[1]Department of Mechanical Engineering, University of Hyogo, 2167 Shosha, Himeji, Hyogo 671-2280, Japan
[2]Course of Aerospace Engineering, Muroran Institute of Technology, 27-1 Mizumoto-cho, Muroran, Hokkaido 050-8585, Japan
[3]Japan Aerospace Exploration Agency, 2-1-1 Sengen, Tsukuba, Ibaraki 305-8505, Japan
[4]Department of Aeronautics and Astronautics, University of Tokyo, 7-3-1 Hongo, Bunkyo-ku, Tokyo 113-8656, Japan
[*]kawanami@eng.u-hyogo.ac.jp
[+]these authors contributed equally to this work

ABSTRACT

This study proposes a one-dimensional droplet model to predict the jet-tip height of a subcooling mixing jet issuing from the bottom of a cryogenic propellant storage tank. Cryogenic liquids, such as liquid hydrogen and liquid oxygen, are used as propellants and oxidants in spacecraft propulsion systems that require long-term storage in a closed tank. However, thermal stratification forms near the gas-liquid interface during long-term storage of cryogens due to heat flowing into the tank from the surrounding environment. In addition, boil-off gas (BOG) is generated from the interface, which causes increased pressure in the tank. To reduce the BOG, it is effective to destroy the thermal stratification by mixing in the cold jet issuing from the bottom of the tank. Ground experiments using FC-72 and water as test fluids are conducted to investigate the behavior of the jet using the proposed one-dimensional spherical droplet model as the tip of the jet. The jet behavior is visualized using the Shadowgraph system and the height of the jet-tip is investigated under various experimental conditions. The proposed model is also verified by comparison with experimental data available in the literature. The results show that the proposed model aligns well with the experimental data.

Introduction

Thermal management technology for a cryogenic propellant storage tank is an important component of future activity planning to achieve long-term space exploration[1–3]. The cryogenic propellant storage tank suffers loss of propellant due to boil-off, which is induced by heat leakage into the tank from the surrounding environment. However, discharging boil-off gas (BOG) is equivalent to the throw energy of the propellant in the environment. Mars missions take an exceedingly long time, so Schaffer and Wenne analyzed the propellant mass fraction and boil-off rate because they have a significant impact on the total stage size[4]. They reported that conservative estimates for these variables could cause the mission to become unfeasible.

The BOG should be released from the tank into space to control the tank pressure within its structural limitations. On the ground, a practical method of depressurization of a cryogenic tank is to directly vent the vapor on the top. However, in a microgravity environment, where the distribution of liquid and vapor in the tank is unknown or not fixed, direct exhaust will likely cause a massive loss of the liquid propellant. A thermodynamic vent system (TVS) that suppresses the rise in temperature and pressure by venting and cooling the fluid in the tank has been effective in reducing the amount of propellant loss due to tank pressure.

TVS is a particularly suitable method for a microgravity environment because the liquid state propellant can be released by discharging the BOG when the position of the gas and liquid is unclear. TVS was first proposed by NASA in the 1990s[5]. Verification tests[6–8] and numerical analyses[9–12] have been conducted to determine its usefulness.

In general, the cryogenic liquid in a tank forms temperature stratification where the temperature near the liquid surface is higher than that of the bulk liquid region due to heat ingress from the outside of the tank[13]. The thermal stratification of the cryogen partially enhances the generation of the BOG and pressurization rate inside the tank. Therefore, destroying the temperature stratification near the gas-liquid interface is considered to be effective for BOG suppression.

Mixing bulk liquid in a tank is one of the most important chemical processing industries. The two common ways to

achieve liquid mixing in a tank are impeller stirred and jet mixed tanks[14]. Axial jet mixing is generally used for cryogenic fluid management in space.

Imai *et al.*[15–18] conducted verification experiments on the TVS by jet mixing a simulated liquid (LN2) on the ground. Subcooled mixing jets were supplied under vent-free conditions, and it was possible to reduce the pressure in the tank and boil-off rate by approximately 98%. However, depending on the liquid level and supply flow rate of the mixing jet, it was found that the tip of the mixing jet could not reach the free surface and the reduction of tank pressure could not be achieved. These results showed the effectiveness of jet mixing for reducing the BOG and the importance of using an appropriate jet flow rate at the actual TVS.

To analyze the behavior of axial jet mixing of ethanol in a container, Aydelott examined the liquid flow patterns that resulted from the axial-jet mixing of ethanol in 10 cm diameter spherical and cylindrical containers under zero-, reduced-, and normal-gravity conditions[19,20]. He reported that four distinct liquid flow patterns were observed: dissipation of the liquid jet in the bulk-liquid region, geyser formation, liquid collection at the end of the tank opposite the jet exit, and complete circulation of the liquid along the tank walls. Dimensionless parameters were developed that characterized the observed liquid flow patterns and bulk-liquid mixing phenomena.

Prediction of the geyser form caused by axial jet mixing was performed using computational fluid dynamics (CFD)[21–23]. The CFD studies were developed from the same set of experimental data[19,20] using the jet-Weber number, jet-Bond number, and tank-Bond number to describe the geyser formation and predict geyser height. These CFD simulations focused on the geyser form and the deformation behavior of the liquid surface. However, there was no detailed discussion regarding the jet behavior below the liquid surface, which is important for suppressing the BOG.

Breisacher *et al.* investigated the effects of tank scale by performing two-dimensional axisymmetric CFD simulations of existing ground-based axial jet mixing experiments using two tank sizes differing by a factor of ten[24]. This was done to understand the control of tank pressure and reduction of thermal stratification in a large-scale tank using axial jet mixing.

The large tank size was equivalent to the Ares V Earth Departure Stage (EDS) LH_2 tank. With the modeling parameters determined from the water tank simulations, CFD simulations were performed based on the mixing histories of an EDS class propellant tank using a jet mixer to control thermal stratification. The simulation results showed a wide variety of mixing behaviors and were consistent with those expected from the use of similar parameters. These CFD simulations were very effective, however, predicting the mixed jet behavior with lower computational cost is necessary for wide application. Results of past research showed that the tip position of the mixing jet was extremely important for BOG suppression.

The authors previously reported the behavior of a mixing jet using a visualization method and described the tip of the jet with a simple one-dimensional model without heat transfer[25]. In this simple dynamic model, a single spherical droplet was assumed as the tip of the jet, and an equation of motion (EOM) was applied to the droplet in the bulk liquid. The results of the analysis model were compared with experimental data from the Shadowgraph system. The trend of the tip velocity with time was well-matched except for the early stage within 0.2 sec. The highest positions of the tip for the analytical model were roughly the same as those of the experimental data.

This study proposes an extension of the authors' previous simple one-dimensional droplet model to include not only the bulk liquid, but the regions of the liquid surface and gas phase above the surface. In addition, a comparison is conducted with the experimental results of other research regarding the maximum height of the tip of the cooling jet to further examine the validity of the proposed model.

Experiment

Experimental apparatus

Figure 1 shows the experimental set-up for the present study.

The main components of the apparatus were a pump (GA-V21.J8FS.A, Micropump), Coriolis flow meter (FD-SS02A, Keyence Co.), reservoir tank for the cooling jet, test tank, pressure sensor (AP-C30, Keyence Co.), two solenoid valves (VX2 Series, SMC Co.), and thermocouples. The test tank was made of SUS306, and the internal height, width, and depth dimensions of the tank were 150, 75, and 26 mm, respectively. Thus, the volume of the tank was 292.5 mL. Quartz glass windows were installed on the tank to observe the internal flow behavior. Four ceramic heaters were mounted on each side wall of the tank to warm up the liquid in the tank. The jet nozzle was located at the center of the tank bottom. The nozzle shape was a circular tube with inner diameter D of 0.5 mm. The nozzle projected 10 mm upward from the bottom of the tank. Therefore, the distance from the inlet of the jet nozzle to the top wall of the tank h_{tank} was 140 mm.

Three groups of eight thermocouples, each with a diameter of 1.0 mm, were arranged at both sides of the center of the tank and near the tank wall to measure the temperature distribution along the axial direction inside the tank. The interval between each thermocouple in the same line was 20 mm. This study focused on the flow behavior during jet injection, so the temperature data obtained by these thermocouples are not presented in this paper.

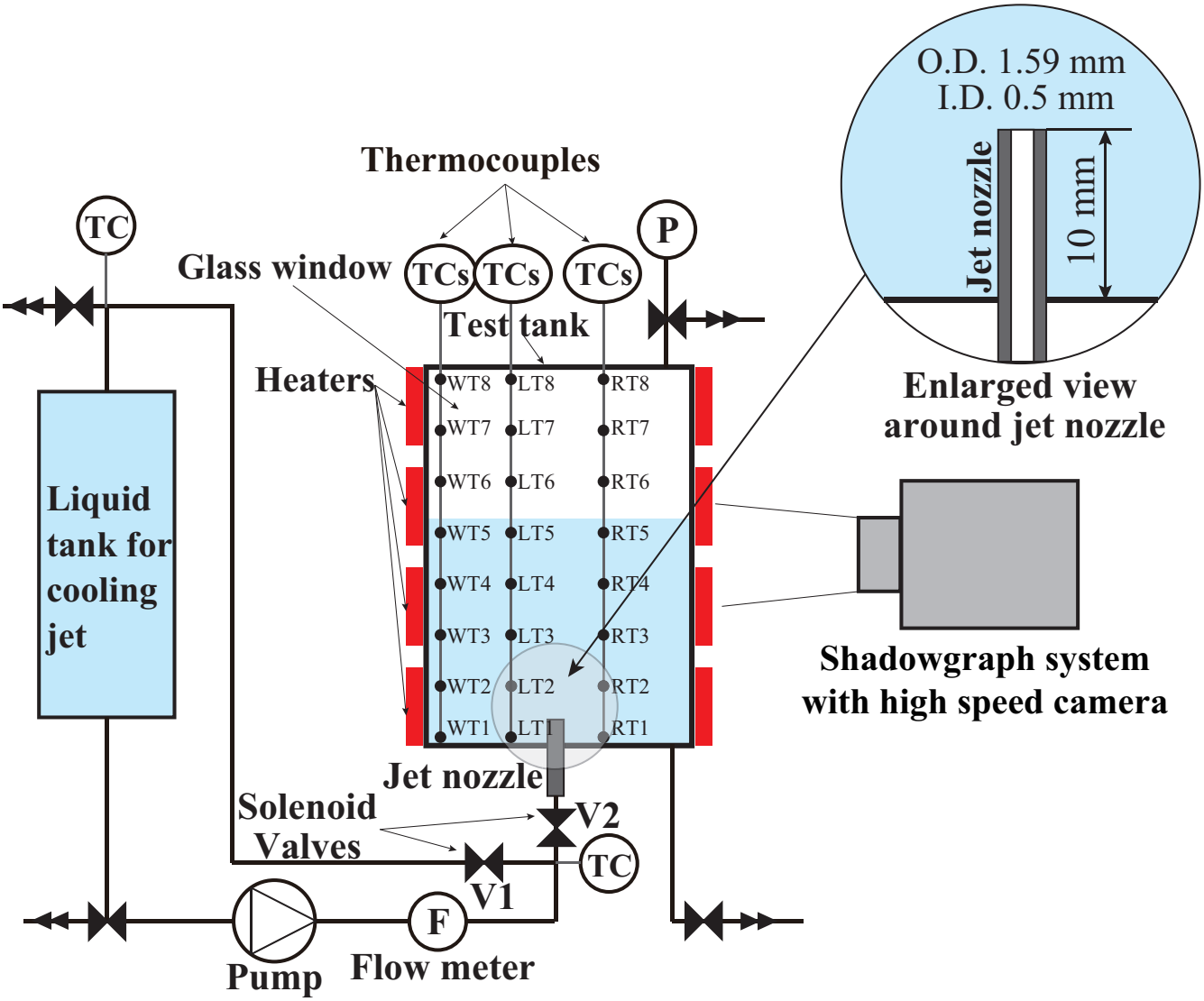

Figure 1. Experimental set-up.

The Shadowgraph system (SS50, KATO KOKEN Co. Ltd.) and a high-speed camera (k8-USB, KATO KOKEN Co. Ltd.) were used to observe the flow behavior. The frame rate and shutter speed of the high-speed camera were set to 60 fps and 1/3000 s, respectively. The field of view of the camera was 48 mm in diameter. The camera was moved up or down in the case where the jet behavior was not observed in the view, and experiments were conducted twice under the same conditions. All data were collected using a data logger (LR8400/LR8501, HIOKI E.E. Co.) with a measurement speed of 10 Hz.

Experimental procedures and conditions

The liquid in the test tank was warmed with a heater on the side wall of the tank before the experiment and the liquid temperature was maintained at 30 K higher than ambient temperature. The temperature of the cooling jet was maintained at ambient temperature. First, the liquid for the cooling jet flowed in the loop by opening the V1 valve and closing the V2 valve. The flow rate corresponding to the experimental condition was controlled by the pump. After receiving the start signal, the V1 valve was closed, the V2 valve was opened, and the cooling jet was issued from the nozzle for 2∼10 seconds. Subsequently, the cooling liquid flowed into the reservoir tank again by opening the V1 valve and closing the V2 valve. The flow behavior was captured with a high-speed camera and the measurement data were synchronized with the high-speed camera by turning off the LED lighting with the start signal.

Experimental conditions were as follows; the temperature difference between the subcooling jet and bulk liquid in the tank ΔT was 10∼30 K, the flow rate of the subcooling jet $\dot{m}_j$ was 3.0 ∼110 mL/min, the initial height of the bulk liquid in the tank

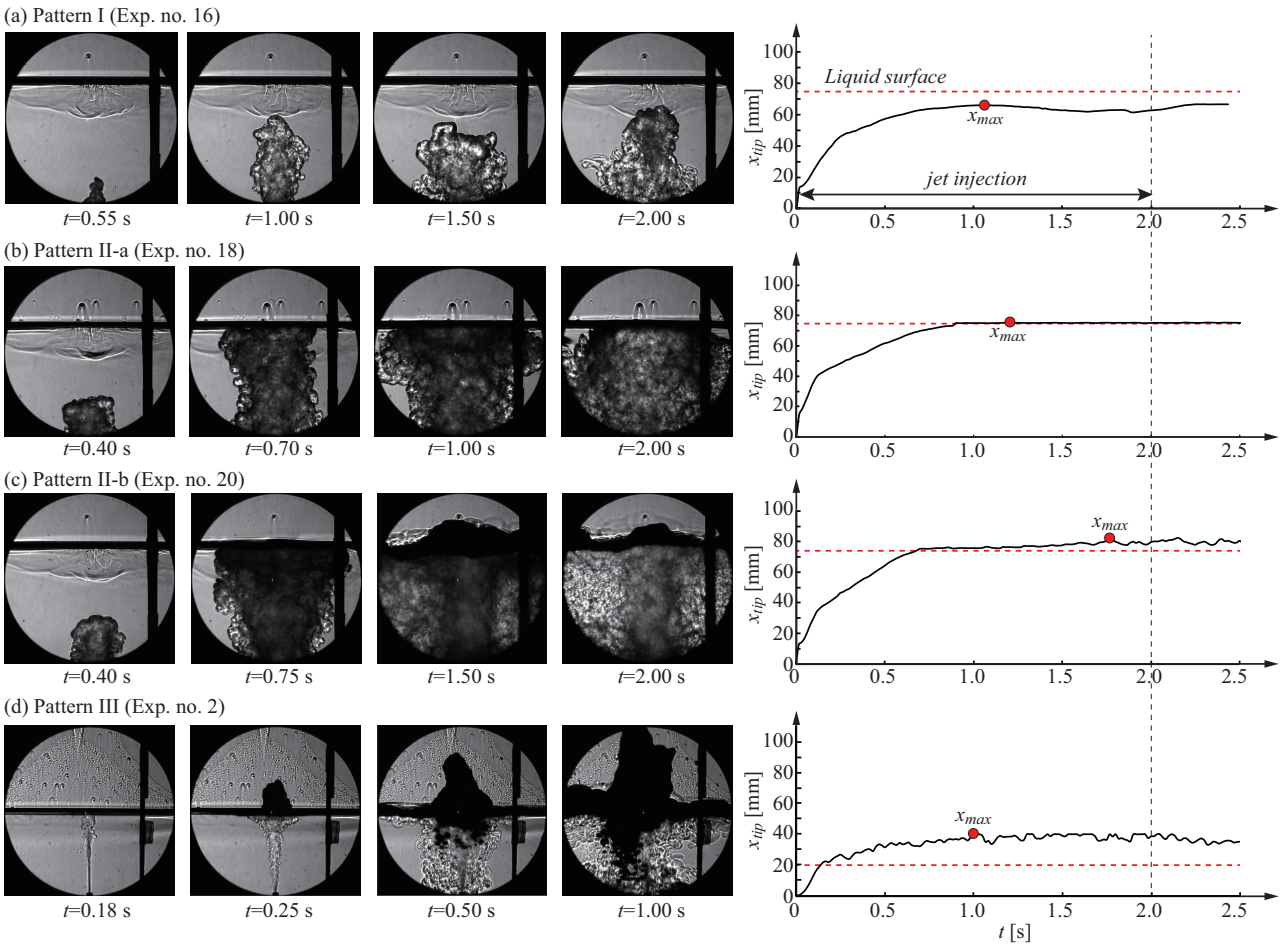

Figure 2. Typical jet behavior and time transitions of the tip position of the jet.

h_{bulk} was 20∼125 mm, and the duration of the cooling jet injection t_{inj} was 2∼10 s. FC-72 and water were used as test fluids, and the same liquid was used for the cooling jet and bulk liquid in the test tank for each experiment. FC-72 has a low surface tension and is used on the assumption that the cryogenic fluids are liquid oxygen and liquid hydrogen. All of the experimental conditions (80 cases) are listed in Table S-1 (See Supplementary S-1).

Experimental results

Four typical flow patterns of jet behavior were observed in the experiment, as shown in Fig. 2.

The cooling jet did not reach the liquid surface and gradually diffused into the bulk liquid for low jet flow rate conditions, as shown in Fig. 2(a). This flow pattern (Pattern I) was not efficient for mixing the bulk liquid.

The jet reached the liquid surface by increasing the jet flow rate, as shown in Fig. 2(b). This jet spread horizontally along the liquid surface and gradually descended into the bulk liquid due to the density difference with respect to the bulk liquid. The surface remained stable when the jet flow rate was lower. However, agitation from the jet was observed near the surface when the flow rate was increased, as shown as Fig. 2(c). These two flow behaviors are classified as Pattern II because the mixing effect for bulk liquid increased with an increase in the jet flow rate. It is unnecessary to clearly distinguish these behaviors, but they have been classified as Pattern II-a and II-b, as shown in Figs. 2(b) and (c), respectively.

The behavior shown in Fig. 2(d) is observed only under the condition of an extremely low height of bulk liquid. In this case, the jet that caused the entrainment of the bulk liquid penetrated the surface, forming a geyser-like flow pattern. This flow pattern has previously been reported under microgravity conditions[19,26]. Here, it was observed that this unique flow pattern (Pattern III) also appeared under terrestrial conditions. The mixing effect of Pattern III was lower than that of Pattern II because the jet consumed part of the energy in the vertical direction to break through the liquid surface. Flow patterns observed for all experimental cases are listed in Table S-1.

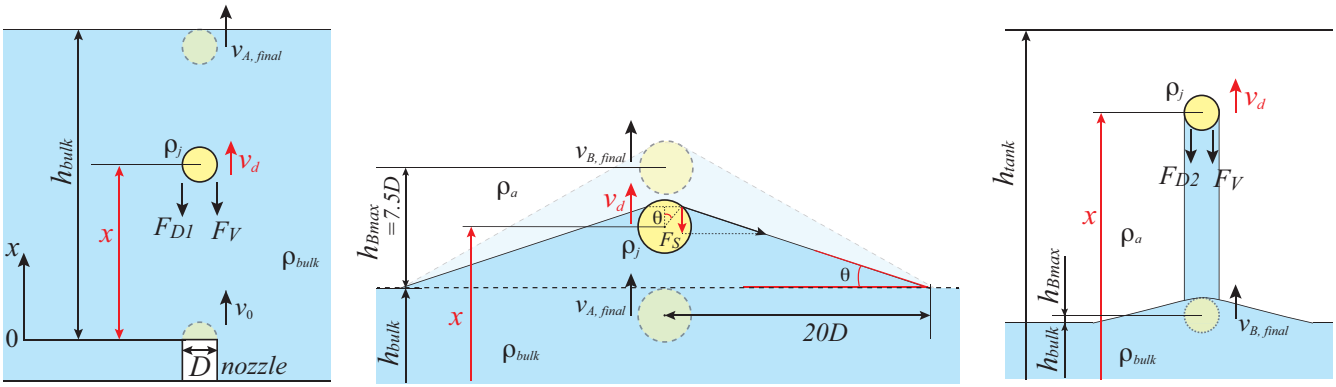

(a) Region A (b) Region B (c) Region C

Figure 3. Schematic of the one-dimensional droplet model.

One-dimensional droplet model for prediction of the jet-tip position

In this study, the tip of the jet assumes a rigid spherical droplet with the same diameter as the nozzle inner diameter D. The position of the jet-tip in the x direction is predicted by a simple one-dimensional equation of motion (EOM) for the droplet, expressed as:

$$m_d \frac{dv_d}{dt} = F \tag{1}$$

where m_d is the mass of the droplet, v_d is the velocity of the droplet in the x direction, t is time, and F denotes the force acting on the droplet. m_d is expressed by the nozzle diameter D and jet liquid density ρ_j, expressed as:

$$m_d = \frac{4\pi (D/2)^3 \rho_j}{3}. \tag{2}$$

Here, the EOM for the droplet is considered by dividing the force acting on the droplet into three regions: the bulk liquid, vicinity of the gas-liquid interface, and gas space.

Region A: Bulk liquid region ($0 \le x \le h_{bulk} - D/2$)

In the bulk liquid region (Region A), the forces acting on the droplet are gravitational F_V and resistance F_{D1}. The latter is applied to the droplet from the surrounding liquid, as shown in Fig. 3(a).

The EOM in Region A is expressed as:

$$m_d \frac{dv_d}{dt} = F_{D1} + F_V. \tag{3}$$

Here, the droplet is assumed as a rigid sphere, so F_{D1} is expressed as:

$$F_{D1} = -\alpha \frac{C_D \rho_{bulk} S}{2} v^2 \tag{4}$$

where S is the cross area of the droplet $\pi D^2/4$, ρ_{bulk} is the density of bulk liquid. C_D is the coefficient of resistance depending on the Reynolds number, $Re = \rho_j v_d D/\mu_d$, which is expressed as[27]:

$$C_D = \frac{24}{Re} + \frac{2.6\left(\frac{Re}{5.0}\right)}{1+\left(\frac{Re}{5.0}\right)^{1.52}} + \frac{0.411\left(\frac{Re}{2.63\times10^5}\right)^{-7.94}}{1+\left(\frac{Re}{2.63\times10^5}\right)^{-8.00}} + \frac{0.25\left(\frac{Re}{10^6}\right)}{1+\left(\frac{Re}{10^6}\right)}. \tag{5}$$

μ_d in the Re is viscosity of the droplet. F_V results from the density difference between the cooling jet and bulk liquid, expressed as:

$$F_V = -(\rho_j - \rho_{bulk}) V g, \tag{6}$$

where V is the volume of the droplet and g is the gravitational acceleration. The fitting parameter α in Eq. (4) is introduced to consider the difference between this simple analytical model and the actual phenomena, such as added mass caused by the flow around the sphere droplet[28] and the expanding and diffusing of the jet. The form of α in this study is expressed as:

$$\alpha = \frac{\rho_j - \rho_{bulk}}{\rho_{bulk}}. \tag{7}$$

Therefore, the EOM in this region is expressed as:

$$\frac{dv_d}{dt} = -\frac{3\alpha C_D \rho_{bulk}}{4\rho_j D} v_d^2 - \frac{\rho_j - \rho_{bulk}}{\rho_j} g. \tag{8}$$

By solving the EOM, the droplet velocity v_d in time can be determined as a function of time, and is expressed as:

$$v_d = \sqrt{\frac{B}{A}} \tan\left[-t\sqrt{AB} + \tan^{-1}\left(v_0\sqrt{\frac{A}{B}}\right)\right]. \tag{9}$$

The detailed solution process of substituting Eq. (8) into Eq. (9) is described in Supplementary S-2. Therefore, the droplet position x in time was obtained using a sequential calculation of the velocity, expressed as:

$$x_t = x_{t-dt} + v_d dt, \tag{10}$$

where x_{t-dt} is the position of the droplet at time $t - dt$. The constant values A and B in Eq. (9) are respectively expressed as:

$$A = \frac{3\alpha C_D \rho_{bulk}}{4\rho_j D} and \quad B = \frac{\rho_j - \rho_{bulk}}{\rho_j} g. \tag{11}$$

The final velocity and position in Region A are $v_{A,final}$ and $x_{A,final}$, respectively. $x_{A,final}$ is equal to $h_{bulk} - D/2$.

Region B: Interfacial region ($h_{bulk} - D/2 < x \leq h_{bulk} + h_{Bmax}$)

The surface tension force F_s is the dominant force acting on the droplet from the interface in the Region B vicinity, as show in Fig.3(b). This region is defined as the location of the droplet from $h_{bulk} - D/2$ to $h_{bulk} + h_{Bmax}$. h_{Bmax} was determined from the results of the experimental images obtained using the Shadowgraph system and set to $7.5D$. F_S can be derived from the following equation:

$$F_S = -\pi D \sigma \sin^2\theta, \tag{12}$$

where σ is the surface tension of the bulk liquid as a function of the temperature at the interface[29], expressed as:

$$\sigma = \sigma_0 \left(1 - \frac{T}{T_c}\right)^{\frac{11}{9}}. \tag{13}$$

Here, σ_0 is a constant value of 0.01447 for FC-72, and T_c is the critical temperature. The surface tension of water is calculated using REFPROP ver. 8 software. θ in Eq. (12) is the angle between the interface and the top of the droplet, as shown in Fig.3(b). From the experimental images, liquid entrainment was observed when the droplet passed through the liquid surface. Thus, the length of the entrainment was set to $20D$. In Eq. (12), θ can be solved using the following equation:

$$x_t - h_{bulk} = 20D\tan\theta - \frac{D/2}{\cos\theta}. \tag{14}$$

Therefore, the EOM in Region B can be solved and is expressed as:

$$\frac{dv_d}{dt} = -\frac{3\sigma\sin^2\theta}{2\rho_j (D/2)^2} \tag{15}$$

The velocity and position of the droplet in this region are respectively expressed as:

$$v_d = -\frac{3\sigma\sin^2\theta}{2\rho_j (D/2)^2} t + v_{A,final} \tag{16}$$

and

$$x_t = x_{t-dt} + v_d dt. \tag{17}$$

The final velocity and position in this region were $v_{B,final}$ and $x_{B,final}$, respectively. $x_{B,final}$ is equal to h_{Bmax}.

Region C: Gas region ($h_{bulk} + h_{Bmax} < x \leq h_{tank} - D/2$)

After the droplet goes through the gas-liquid interfacial region (Region B), the droplet entrainment of the bulk liquid from the gas-liquid interface proceeded into the air (Region C), as shown in Fig. 3(c). The EOM in Region C is expressed as:

$$m_d \frac{dv_d}{dt} = F_{D2} + F_V. \tag{18}$$

where F_{D2} is the drag force acting on the droplet in the vapor of the bulk liquid and F_V is the body force of the droplet and entrainment liquid.

$$F_{D2} = -\frac{C_D \rho_a S}{2} v_d^2 \tag{19}$$

where C_D is the same as in Eq. (5).

$$F_V = -\rho_j g \left[\frac{2}{3}\pi r^3 + \pi r^2 \left(x_{t-dt} - h_{bulk} - h_{Bmax} \right) \right]. \tag{20}$$

Therefore, the EOM in Region C is now expressed as:

$$\frac{dv_d}{dt} = -\frac{3C_D \rho_a}{4\rho_j D} v_d^2 - \frac{D + 3x_{t-dt} - 3h_{bulk} - 3h_{Bmax}}{2D} g. \tag{21}$$

By solving Eq. (21), v_d and x_t in Region C can be obtained and are respectively expressed as:

$$v_d = \sqrt{\frac{B'}{A'}} \tan \left[-t\sqrt{A'B'} + \tan^{-1} \left(v_{B,final} \sqrt{\frac{A'}{B'}} \right) \right], \tag{22}$$

and

$$x_t = x_{t-dt} + v_d dt. \tag{23}$$

Here A' and B' are respectively expressed as:

$$A' = \frac{3C_D \rho_a}{4\rho_j D}, \quad B' = \frac{D + 3x_{t-dt} - 3h_{bulk} - 3h_{Bmax}}{2D} g. \tag{24}$$

Comparison of the proposed model and experimental results

Comparison of the present experiment

First, the proposed one-dimensional model was compared with the previously presented experimental results. The transition of the jet-tip height derived from the model is shown in Fig. 4(a).

The model was calculated under three flow pattern conditions at a liquid height of 75 mm, which represent Exp. nos. 16, 18, and 20 in Table S-1. The calculation was stopped when the tip of the jet reached the maximum height, which corresponded to the velocity of the x-direction reaching zero.

The maximum jet-tip height calculated by the model under the same conditions as in Exp. no. 16 was 65.53 mm, which is located in the bulk liquid. Thus, this was classified as Pattern I. The model analytical heights under the conditions of Exp. nos. 18 and 20 were 78.25 and 81.02 mm, respectively. The still images at the maximum height of the jet for each experiment are shown in Fig. 4(b). The x-axis in the image is the center line of the nozzle, and the x-positions of these images coordinate with the x-coordinates of Fig. 4(a). The maximum height of Pattern I was 65.6 mm, which almost aligns with the model results. In the case of Pattern II-a, the tip height was the same as that of the liquid surface, 75 mm. However, the height in the model analysis was approximately 78 mm, which was slightly higher than the liquid level. Region B in the model is narrow, extending from the liquid surface to 4 mm above it. This region corresponds to the Pattern II-a experimental result. When the tip of the jet exceeded this region, the flow pattern shifted to II-b or III. As aforementioned, the maximum height of II-b using the model was 81.02 mm. This case is classified as Pattern II-b because its height exceeded that of Region B. The maximum height in the experiment was 86.02 mm, which is the condition in Exp. no. 20. This height is slightly higher than the model result. It was difficult to determine from the model analysis whether the jet behavior was classified as Pattern II-b or III. However, the maximum heights of the jet-tip calculated by the proposed simple model, x_{max_model}, aligned well with the experimental data, x_{max_exp}, as shown in Fig. 5.

The mean absolute error (MAE) between the proposed model and experimental data was 4.04. This result indicates that the one-dimensional droplet model proposed here has sufficient accuracy to predict the maximum height of the jet-tip, and the flow pattern is sufficiently predictable.

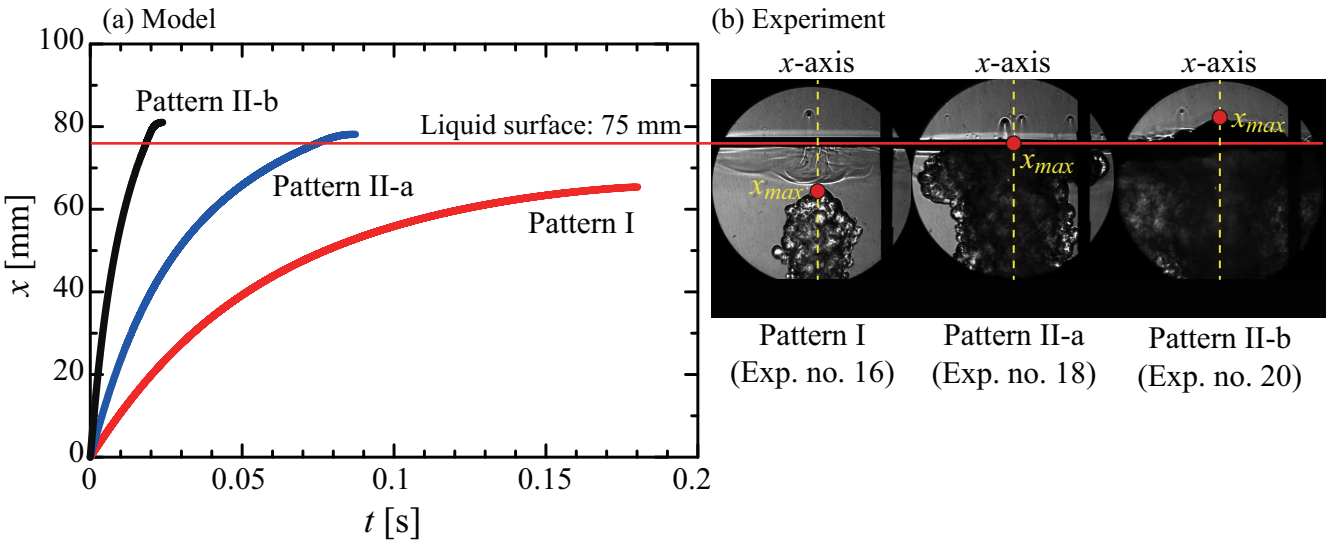

Figure 4. Transition of the typical jet-tip height derived from the proposed model for Patterns I, II-a, and II-b.

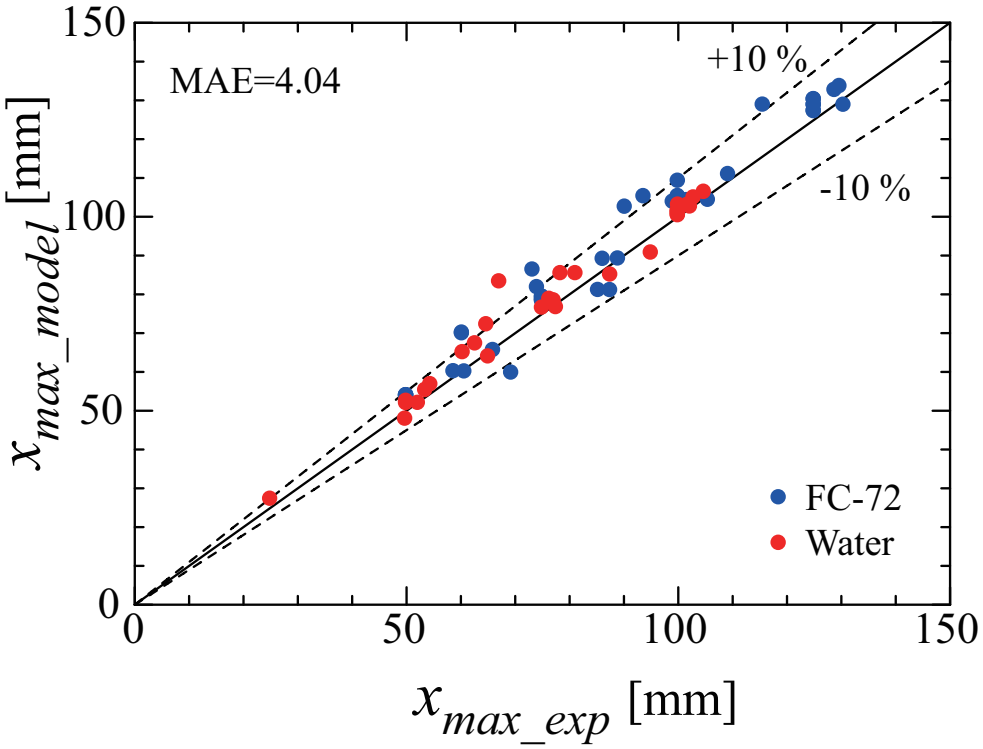

Figure 5. Comparison of maximum heights of the jet-tip.

Comparison with experimental results in other literature 1: immiscible liquids

Geyer's experiments using various nozzle diameters from 2.4 to 12 mm were carried out by injecting a jet of dyed fresh water through a nozzle into the base of a cylindrical tank containing rapeseed oil[26]. Three different flow patterns were categorized based on the visualization results of the jet flow: Type I, II, and III. Type I was characterized by an approximately constant jet height within the range of experimental error of the observation. In the case of Type II flow behavior, the jet height was not constant but varied continuously with time. As a result, Type II formed a pulsating flow. Type III behavior was characterized by the jet initially penetrating upward into the ambient fluid. When it reached maximum height, the accumulated jet fluid formed a cap shape at the top of the jet. It was concluded that a stable jet shape was not formed except for Type III. A comparison of the

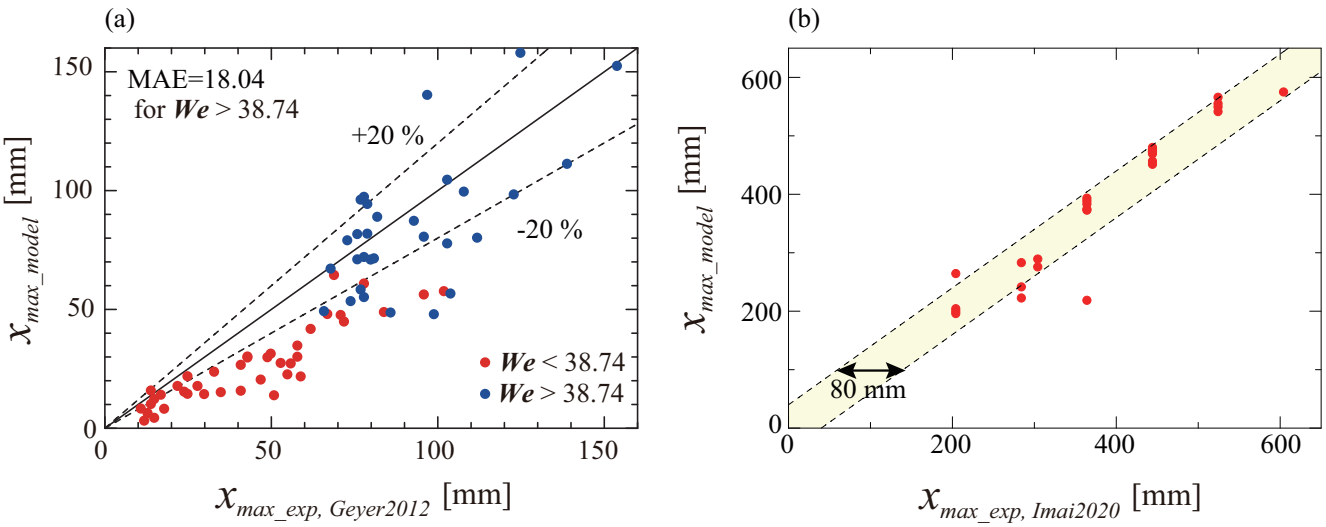

Figure 6. Comparison of the proposed model and experimental data from other literature.

maximum tip height of the jet predicted by the proposed model and Geyer's experimental results, $x_{max\_exp,Geyer2012}$, under the conditions of $We > 38.74$ in Type III, is shown in Fig. 6(a). We was defined as $\rho_j v_j^2 d/\sigma$ in Ref.[26][26].

For $We < 38.74$, the jet shape and flow did not reach a steady state, indicating that the difference between the model and experimental data was large. When the We number exceeded 38.74, the tendency of the jet-tip height predicted by the proposed one-dimensional model aligned with the experimental data. The MAE between the experimental data and model analysis was 18.04 when $We > 38.74$.

Comparison with experimental results in other literature 2: cryogenic fluid

In a study by Imai, the experimental setup consisted of a test tank, vacuum chamber, pre-cooler to maintain the mixing jet in a subcooled state, and two LN2-storage tanks[17]. The mixing jet was pre-cooled in a coiled tube in the pre-cooler upstream of the mixing jet inlet at the bottom of the test tank. The mass flow rate of the mixing jet was measured using a Coriolis flow meter. The inlet of the mixing jet, which had a diameter of 10 mm, was projected 100 mm upward from the bottom of the tank. The test tank was made of stainless steel, and there was no window for observing the flow behavior. Nine platinum resistance temperature sensors were installed on the center axis and side wall, and four others were placed on the bottom of the test tank. The distance between each temperature sensor on the center axis and side wall was 80 mm. Therefore, the height of the cooling jet-tip could be determined from the temperature drop of the sensors. In other words, the height of the jet could only be known at intervals of 80 mm.

A comparison of the maximum tip height of the jet predicted by the proposed model and Imai's experimental results is shown in Fig. 6(b). Please note that the height of the jet-tip was from the inlet of the jet nozzle to the tip position. Therefore, the jet-tip position in Imai's experiment $x_{max\_exp,Imai2020}$ is actually 0.1 m less from the sensor locations because the jet was located 0.1 m above the bottom of the tank. As mentioned above, $x_{max\_exp,Imai2020}$ is derived from the temperature sensor data in the experimental device. Therefore, detection accuracy cannot be less than 80 mm, which is the distance between the temperature sensors. It was found that the proposed model was suitable for predicting the height of the jet-tip. If a plot was in the yellow area of Fig. 6(b), the model was able to predict the experimental data.

Conclusions

Cryogenic fluids are used as propellants and oxidants in the propulsion systems of spacecraft for future long-term space explorations. For cryogenic fluid management in space, a TVS is a key technology to suppress a rise in pressure due to the BOG in the propellant tank. It is effective to destroy the temperature stratification near the interface to reduce the BOG. Ground experiments were conducted to investigate the behavior of the axial-jet mixing, which is a key technology of TVS. In addition, a one-dimensional dynamic model was constructed using a single-sphere droplet as the tip of the jet. The mixing jet behavior was experimentally visualized using the Shadowgraph system, and the height of the jet-tip was investigated by varying the bulk liquid volume in the tank, jet flow rate, jet temperature, injection duration, and types of liquid. Water and FC-72 were used for the test fluids. The main conclusions of this study are as follows.

(i) Shadowgraph images of the jet behavior demonstrated four typical flow patterns of jet behavior in the experiment: Pattern I, Pattern II-a, Pattern II-b, and Pattern III. Pattern III, where the jet caused the entrainment of the bulk liquid and penetrated the surface to form a geyser-like flow pattern, was observed only when the height of the bulk liquid was extremely low under terrestrial conditions.

(ii) The proposed model aligned well with the experimental data. The MAE between the model and experimental data was 4.04.

(iii) The results of the proposed model were compared to experimental data from other literature. The proposed one-dimensional droplet model was shown to have sufficient accuracy to predict the maximum height of the jet-tip, and the flow pattern was sufficiently predictable.

References

1. Chato, D. J. Low gravity issues of deep space refueling. In *Proc. 43th AIAA Aerospace Sciences Meeting and Exhibit*, AIAA–2005–1148, DOI: https://doi.org/10.2514/6.2005-1148 (2005).
2. Motil, S. M. & Meyer, M. L. Cryogenic fluid management technologies for advanced green propulsion systems. In *Proc. 45th AIAA Aerospace Sciences Meeting and Exhibit*, AIAA–2007–343, DOI: https://doi.org/10.2514/6.2007-343 (2007).
3. Muratov, C. B., Osipov, V. V. & Smelyanskiy, V. N. Issues of long-term cryogenic propellant storage in microgravity. NASA/TM–2011–215988 (2011).
4. Schaffer, M. & Wenne, C. A study of cryogenic propulsive stages for human exploration beyond low earth orbit. In *Proc. Global Space Exploration Conf.*, GLEX–2012.05.1.4x12564 (2012).
5. Lak, T. & Wood, C. Cryogenic fluid management technologies for space transportation : zero g thermodynamic vent system final report. NASA CR-193981 (1994).
6. Hasan, M. M., Lin, C. S., Knoll, R. H. & Bentz, M. D. Tank pressure control experiment: Thermal phenomena in microgravity. NASA TP–3564 (1996).
7. Wang, B. *et al.* Performance of thermodynamic vent system for cryogenic propellant storage using different control strategies. *Appl. Therm. Eng.* **126**, 100–107, DOI: https://doi.org/10.1016/j.applthermaleng.2017.07.158 (2017).
8. Bae, J., Yoo, J., Jin, L. & Jeong, S. Experimental investigation of passive thermodynamic vent system (tvs) with liquid nitrogen. *Cryogenics* **89**, 147–156, DOI: https://doi.org/10.1016/j.cryogenics.2017.11.001 (2018).
9. Barsi, S. & Kassemi, M. A numerical study of tank pressure control in reduced gravity. In *Proc. 44th AIAA Aerospace Sciences Meeting and Exhibit*, AIAA 2006–936, DOI: https://doi.org/10.2514/6.2006-936 (2006).
10. Barsi, S. & Kassemi, M. Numerical and experimental comparisons of the self-pressurization behavior of an lh2 tank in normal gravity. *Cryogenics* **48**, 122–129, DOI: https://doi.org/10.1016/j.cryogenics.2008.01.003 (2008).
11. Kassemi, M. & Kartuzova, O. Effect of interfacial turbulence and accommodation coefficient on cfd predictions of pressurization and pressure control in cryogenic storage tank. *Cryogenics* **74**, 138–153, DOI: https://doi.org/10.1016/j.cryogenics.2015.10.018 (2016).
12. Kassemi, M., Kartuzova, O. & Hylton, S. Validation of two-phase cfd models for propellant tank self-pressurization: Crossing fluid types, scales, and gravity levels. *Cryogenics* **89**, 1–15, DOI: https://doi.org/10.1016/j.cryogenics.2017.10.019 (2018).
13. Kang, M., Kim, J., You, H. & Chang, D. Experimental investigation of thermal stratification in cryogenic tanks. *Exp. Therm. Fluid Sci.* **96**, 371–382, DOI: https://doi.org/10.1016/j.expthermflusci.2017.12.017 (2018).
14. Bumrungthaichaichan, E. A review on numerical consideration for computational fluid dynamics modeling of jet mixing tanks. *Korean J. Chem. Eng.* **33**, 3050–3068, DOI: https://doi.org/10.1007/s11814-016-0236-x (2016).
15. Imai, R., Kawanami, O., Umemura, Y. & Himeno, T. Study on break of thermal stratification in container targeted to thermodynamic vent system for future spacecraft. *IOP Conf. Ser.: Mater. Sci. Eng.* **502**, 012082, DOI: https://doi.org/10.1088/1757-899x/502/1/012082 (2019).
16. Imai, R., Nishida, K., Kawanami, O., Umemura, Y. & Himeno, T. Basic study on thermodynamic vent system in propulsion system for future spacecraft. *Microgravity Sci. Technol.* **32**, 339–348, DOI: https://doi.org/10.1007/s12217-019-09768-w (2020).

17. Imai, R., Nishida, K., Kawanami, O., Umemura, Y. & Himeno, T. Ground based experiment and numerical calculation on thermodynamic vent system in propellant tank for future cryogenic propulsion system. *Cryogenics* **109**, 103095, DOI: https://doi.org/10.1016/j.cryogenics.2020.103095 (2020).

18. Nishida, K., Imai, R., Kawanami, O., Umemura, Y. & Himeno, T. Ground-based experiment on reducing boil-off gas by jet mixing for future cryogenic propulsion system. *Int. J. Microgravity Sci. Appl.* **38**, 380102, DOI: https://doi.org/10.15011/jasma.38.1.380102 (2021).

19. Aydelott, J. C. Axial jet mixing of ethanol in cylindrical containers during weightlessness. NASA TP-1487 (1979).

20. Aydelott, J. C. Modeling of space vehicle propellant mixing. NASA TP-2107 (1983).

21. Hochstein, J. I., Gerhart, P. M. & Aydelott, J. C. Computational modeling of jet induced mixing of cryogenic propellants in low-g. NASA TM-83703, DOI: https://doi.org/10.2514/6.1984-1344 (1984).

22. Hochstein, J. I., Marchetta, J. G. & Thornton, R. J. Microgravity geyser and flowfield prediction. *J. Propuls. Power* **24**, 104–110, DOI: https://doi.org/10.2514/1.26235 (1979).

23. Marchetta, J. G. & Benedetti, R. H. Simulation of jet-induced geysers in reduced gravity. *Microgravity Sci. Technol.* **22**, 7–16, DOI: https://doi.org/10.1007/s12217-008-9095-3 (2010).

24. Breisacher, K. & Moder, J. Computational fluid dynamics (cfd) simulations of jet mixing in tanks of different scales. NASA TM-2010-216749 (2010).

25. Kawanami, O. *et al.* Behavior of subcooling jet injected into a bulk liquid in a tank under normal-and micro-gravity conditions. *Int. J. Microgravity Sci. Appl.* **36**, 360402, DOI: https://doi.org/10.15011/jasma.36.360402 (2019).

26. Geyer, A., Phillips, J. C., Mier-Torrecilla, M., Idelson, S. R. & Oñate, E. Flow behaviour of negatively buoyant jets in immiscible ambient fluid. *Exp. Fluids* **52**, 261–271, DOI: https://doi.org/10.1007/s00348-011-1217-9 (2012).

27. Morrison, F. A. *An Introduction to Fluid Mechanics* (Cambridge University Press, UK, 2013).

28. Wakaba, L. & Balachandar, S. On the added mass force at finite reynolds and acceleration numbers. *Theor. Comput. Fluid Dyn* **21**, 147–153, DOI: https://doi.org/10.1007/s00348-011-1217-9 (2007).

29. Wakaba, L. & Balachandar, S. The principle of corresponding states. *J. Chem. Phys.* **13**, 253–261, DOI: https://doi.org/10.1063/1.1724033 (1945).

Acknowledgements

This research was carried out as part of the "Development of Innovative Thermal Management Technology to Realize Long-term Storage of Cryogenic Propellant" research project, conducted in the Strategic Basic Development Research facility of the Space Engineering Committee in JAXA. We would like to thank Editage (www.editage.com) for English language editing.

Author contributions

O. K. conceived this study, proposed the model, interpreted the results, and wrote the manuscript. K. T. and R. M. performed the experiments and data analysis, and conducted the model calculation. R. I. , Y. U., and T. H. supervised the whole research work. All authors reviewed the manuscript.

Corresponding author

Correspondence to Osamu Kawanami, Tel: +81-79-267-4844, kawanami@eng.u-hyogo.ac.jp

Additional information

Correspondence and requests for materials should be addressed to O. K.

Competing interests

The authors declare no competing interests.

Figure Captions

Figure 1: Experimental set-up.

Figure 2: Typical jet behavior near the liquid surface observed with the Shadowgraph system is shown on the left. Time transitions of the tip position of the jet are shown on the right. The experimental conditions for $\dot{m}_j$ are: (a) 13.5, (b) 32.4, (c)

104.6, and (d) 89.4 mL/min. h_{bulk} = 75 mm and ΔT = 30 K in (a) to (c), h_{bulk} = 20 mm and ΔT = 10 K in (d). t_{inj} = 2 s and FC-72 is used as the test fluid.

Figure 3: Schematic of the proposed one-dimensional droplet model showing the force acting on the droplet in each region. (a) Region A ($0 < x \leq h_{bulk} - D/2$). (b) Region B ($h_{bulk} - D/2 < x \leq h_{bulk} + h_{Bmax}$). (c) Region C ($h_{bulk} + h_{Bmax} < x \leq h_{tank} - D/2$).

Figure 4: Transition of a typical jet-tip height derived from the proposed model for Patterns I, II-a, and II-b. Exp. nos are 16, 18, and 20, respectively. (a) Analytical results of the proposed model. (b) Images when the jet reaches the highest point under each condition.

Figure 5: Comparison of maximum height of the jet-tip for all experimental and analytical results derived by the proposed model.

Figure 6: Comparison of the proposed model and experimental data from other literature. (a) Comparison with Geyer's experimental results[26]. The present model can be applied for the *We* number over 38.74. (b) Comparison with Imai's experimental results[17]. Liquid nitrogen as a test fluid was used in their experiment.

Supplementary Files

This is a list of supplementary files associated with this preprint. Click to download.

- Supplementary1.pdf
- Supplementary2.pdf